Chapter 15

Growth and Characteristics of High-quality InN by Plasma-Assisted Molecular Beam Epitaxy

Chen-Chi Yang, Ikai Lo, Cheng-Hung Shih, Chia-Hsuan Hu, Ying-Chieh Wang, Yu-Chiao Lin, Cheng-Da Tsai, Hui-Chun Huang, Mitch M. C. Chou, Cheng-Chang Yu and Der-Jun Jang

Additional information is available at the end of the chapter

http://dx.doi.org/10.5772/65812

Abstract

The high-quality InN epifilms and InN microdisks have been grown with InGaN buffer layers at low temperatures by plasma-assisted molecular beam epitaxy. The samples were analyzed using X-ray diffraction, scanning electron microscopy, high-resolution transmission electron microscopy, and photoluminescence. The characteristics of the InN epifilms and InN microdisks were studied, and the role of InGaN buffer was evaluated.

Keywords: InN microdisk, InGaN buffer, Molecular beam epitaxy

1. Introduction

III-Nitride semiconductor compounds have been extensively studied for applications in optoelectronic devices, such as solar cells and light emitting diodes (LEDs) [1–5]. The wide direct band-gap gallium nitride (GaN) and aluminum nitride (AlN) compounds, with energy gaps covering the ultraviolet spectrum, are the dominant materials for solid-state lighting devices and have been well studied to date. The molecular beam epitaxy (MBE) technique can be used to grow a thin epifilm in an ultrahigh vacuum (~10^{-10} torr) and low temperature condition [6]. Under such conditions, materials in the effusion cells of the MBE system are heated and they move toward the substrate to form epitaxial high purity films. The low-temperature condition is crucial to grow the compounds with a low volatilized temperature (such as In atom, 650°C). Because of the improvement of InN films grown by MBE, the direct band-gap of the indium

nitride (InN) compound was demonstrated with the value of 0.64 eV rather than 1.9 eV [7, 8]. This important finding indicated that one can tune the band-gap energy to achieve the full-color spectrum (red, green, and blue) devices by changing the III-group alloy ratio without any phosphor. Besides, InN is a high potential material in optoelectronic applications due to its outstanding material properties, such as the smallest effective mass, the highest peak and saturation electron drift velocity, and the largest mobility among the nitride semiconductors [9, 10].

On the other hand, the development of the full-color spectrum micron LED is very important for the high-resolution display. The general method to fabricate micron LED is etching process to reach micro scale. However, it is not easy to downsize to 1–10 μm by etching process. In order to fabricate micron LED, a suitable micron growth base is the top priority. In recent years, the growth and characteristics of InN nanowire on Si (1 0 0) by the vapor-liquid-solid mechanism and on Si (1 1 1) by plasma-assisted molecular beam epitaxy (PA-MBE) were reported [11–13]. The wire diameter was less than 100 nm. In our previous work, we have grown the high-quality self-assembled ***c***-plane GaN ($0\,0\,0\,1^{-}$) hexagonal microdisks with a diameter of 4 μm on γ-$LiAlO_2$ (LAO) substrates. The diameter of microdisk can be adjusted to optimize the quantum effect for nanodevice applications [5]. Besides, we developed a back process to fabricate an electrical contact for the GaN hexagonal microdisk on a transparent p-type GaN template [14]. Consequently, the InN microdisk provides an opportunity to fabricate the InGaN/GaN microdisk quantum well for the application of full-color micron LED without the sapphire substrate, which is mostly used for the bulk GaN-based quantum wells in commercial LEDs but has a large lattice mismatch with InN [1, 2]. In this chapter, we will show the growth of InN ($0\,0\,0\,1^{-}$) hexagonal thin wurtzite microdisks on the γ-LAO substrate by PA-MBE.

2. High-quality InN epifilms

2.1. InGaN buffer layer

When engineering the band structure of III-nitrides, it is difficult to grow high-quality InN thin film due to the low decomposition temperature of InN (<600°C) and the large lattice mismatch between InN and common substrates (e.g., sapphire or silicon) [15]. Therefore, determining an appropriate substrate for the growth of high-quality InN film is one of the main issues in the fabrication of full-color optoelectronic devices. The lattice mismatch between InN (***a*** = 0.3537 and ***c*** = 0.5704 nm) and sapphire (***a*** = 0.4785 and ***c*** = 1.2991 nm) on the ***c***-plane is about 26.1%.

The initial methods prior to InN growth, including substrate nitridation and buffer layer deposition, have very important effects on the growth of high-quality InN films with a flat surface on a sapphire substrate. Xiao et al. grew InN films with 20 min nitridation and a low-temperature InN (LT-InN) buffer layer. By X-ray diffraction (XRD) and room temperature photoluminescence (PL) analyses, it was found that these InN films grown with LT-InN buffer layer have better quality than those without LT-InN buffer layer [16].

Meanwhile, Saito et al. reported the growth of InN films on sapphire with 1 hour nitridation and low-temperature intermediate InN buffer layers, and they found that the growth

of thicker InN with a uniform surface was very difficult without intermediate layers and the electron mobility was improved by improvement of surface flatness [17]. Besides, Lu et al. studied the effect of an AlN buffer layer on the epitaxial growth of InN on the sapphire substrate by MBE and found that by using the AlN buffer layer, the structural and electrical properties of InN could be greatly improved. It was also found that a thicker AlN buffer layer was preferred when growing the InN epilayer, which could lead to better electrical properties and surface morphology [18]. From these studies, we can find that it is helpful to improve the quality of InN thin films by introducing an appropriate buffer layer. In general, a thick GaN film (>4 μm) can be grown on sapphire substrate (0 0 0 1) to form a GaN template. In this chapter, we will show firstly the high-quality epitaxial growth of InN epifilms on GaN template with an appropriate InGaN buffer layer by PA-MBE system. We designed a series of samples to study the effect of InGaN buffer layer with growth-temperature dependence.

2.2. Growth of InN epifilms

Four samples were grown on 2 inch ***c***-plane (0 0 0 1) Si-doped GaN/sapphire template substrates that consisted of 3.5 μm intrinsic GaN, 65 nm Si-doped AlGaN and 2 μm Si-doped GaN were grown by metal-organic chemical vapor deposition (MOCVD). The InN thin film was grown on the InGaN buffer layer by the PA-MBE system (Veeco Applied-GEN 930) with standard effusion cells for In- and Ga-evaporation and an rf-plasma cell with 450 W for the N_2-plasma source. Before mounting on a holder, the template substrates were cleaned with acetone (5 min), isopropanol (5 min), and de-ionized water (5 min) in an ultrasonic bath, and then dried with nitrogen gas immediately. After the chemical cleaning, the substrates were out-gassed at 750°C for 10 min in the MBE chamber before epitaxial growth. The temperature was defined by a thermal couple equipped at the backside of the substrates. Thereafter, the substrate temperature was decreased down to growth temperatures. The epitaxial growth of GaN was performed on the GaN template at 700°C with a flux ratio N/Ga = 42.9 represented by beam equivalent pressure (BEP) of evaporative III-group sources from standard effusion cell against that of N_2 source from rf-plasma cell [19] and the duration time of the epitaxial growth for all samples was 10 min. Thereafter, the substrate temperature was ramped to growth temperatures with a flux ratio In/Ga = 2.0, and the duration time of the InGaN buffer layer for all samples was 10 min. Four samples were grown under varied temperatures of InGaN buffer layers: 500, 540, 570, and 600°C. Finally, the substrate temperature was ramped down to growth temperature at 410°C with a flux ratio N/In = 40.0 and the duration time of the InN for all samples was 10 min to grow the InN epifilms.

2.3. Analysis of InN epifilms

The *in situ* reflection high-energy electron diffraction (RHEED) was used to monitor the growth of InN epifilms with 15 kV and 14 mA. The structural properties and crystalline preferred orientations were characterized by an X-ray diffractometer (Bede D1) and a field emission transmission electron microscope (FE-TEM; Phillips Tecnai F-20) with an electron voltage of 200 kV. The cross-sectional TEM specimens were prepared by a focus ion beam (FIB; Seiko SII-3050). The FIB was performed with accelerated voltage of 30 kV to cut the samples roughly

and then refined the sample further by accelerated voltage of 5 kV. The surface morphology was evaluated by the field emission scanning electron microscope (FE-SEM; Seiko SII-3050) and the atomic force microscope (AFM; Dimension 3100). AFM images were taken with tapping mode by silicon probe and the scanning data were characterized by software NanoScope (R) III (Digital Instruments, version 5.12r2). The photoluminescence (PL) measurement was carried out by Ti:sapphire laser (Traix-320) with a light source from 808-nm laser and 208 mW power from room temperature (300 K) to 14 K to investigate the optical emission properties of the InN epifilms.

The crystal structure of all samples was characterized by XRD measurements. **Figure 1** shows the XRD results of all samples and indicates that ***c***-plane InN epifilms were epitaxially grown on GaN templates. From the peaks of X-ray diffraction pattern at 2θ = 32.84°, 33.13°, 33.15°, and 33.76°, we estimated the content of indium of $In_xGa_{1-x}N$ on the basis of Vegard's law to be about 52, 43, 42, and 23%, respectively [20]. The peaks at 2θ = 31.22°, 32.97°, 34.57°, and 34.82° were corresponding to the X-ray diffraction patterns from **c**-plane InN (0 0 0 2), In (1 0 1), GaN (0 0 0 2), and Si-doped AlGaN (0 0 0 2), respectively. These peak positions for the X-ray diffraction patterns were obtained by software Quick Graph (version 2.0) with the Asymmetric Double Sigmoidal linear curve fitting. We can observe that the peak of $In_xGa_{1-x}N$ shifts from left to right with the increasing growth-temperature of the InGaN buffer layer. This shows that the content of indium decreases with the increasing growth temperature, and the diffraction of Indium was observed corresponds to In droplet on the surface of sample 3. In order to eliminate the influence of In drops in further measurements, the acid treatment (H_3PO_4:HNO_3:CH_3COOH:H_2O = 50:2:10:9) was employed for sample 3 to remove the In drops on the surface. As compared to other samples, the interference fringes of InN grown on sample 1 exhibit prominent oscillations. Qualitatively, it shows that sample 1 is a very high-quality and layer-by-layer epitaxial growth InN epifilm. **Figure 2(a** and **b)** shows the rocking curve and full-width at half maximum (FWHM) values of the plane of InN (0 0 0 2) and $In_xGa_{1-x}N$ (0 0 0 2), respectively. The FWHM values of the plane of InN (0 0 0 2) grown on samples 1, 2, 3, and 4 are 435.7, 651.5, 682.6, and 777.1 arc-sec,

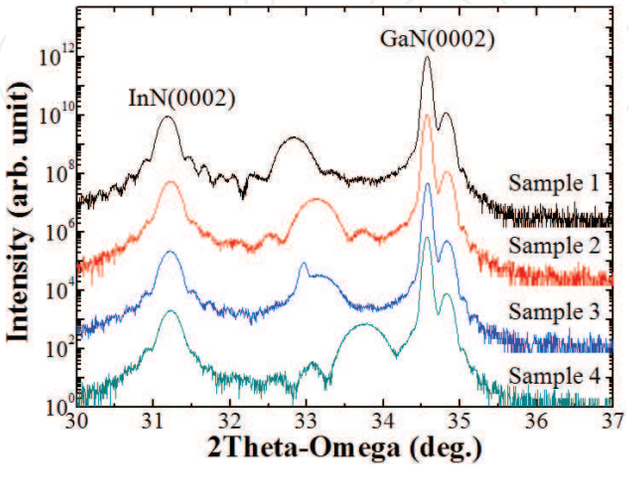

Figure 1. The X-ray 2 Theta-Omega scans of growing samples.

http://dx.doi.org/10.5772/65812

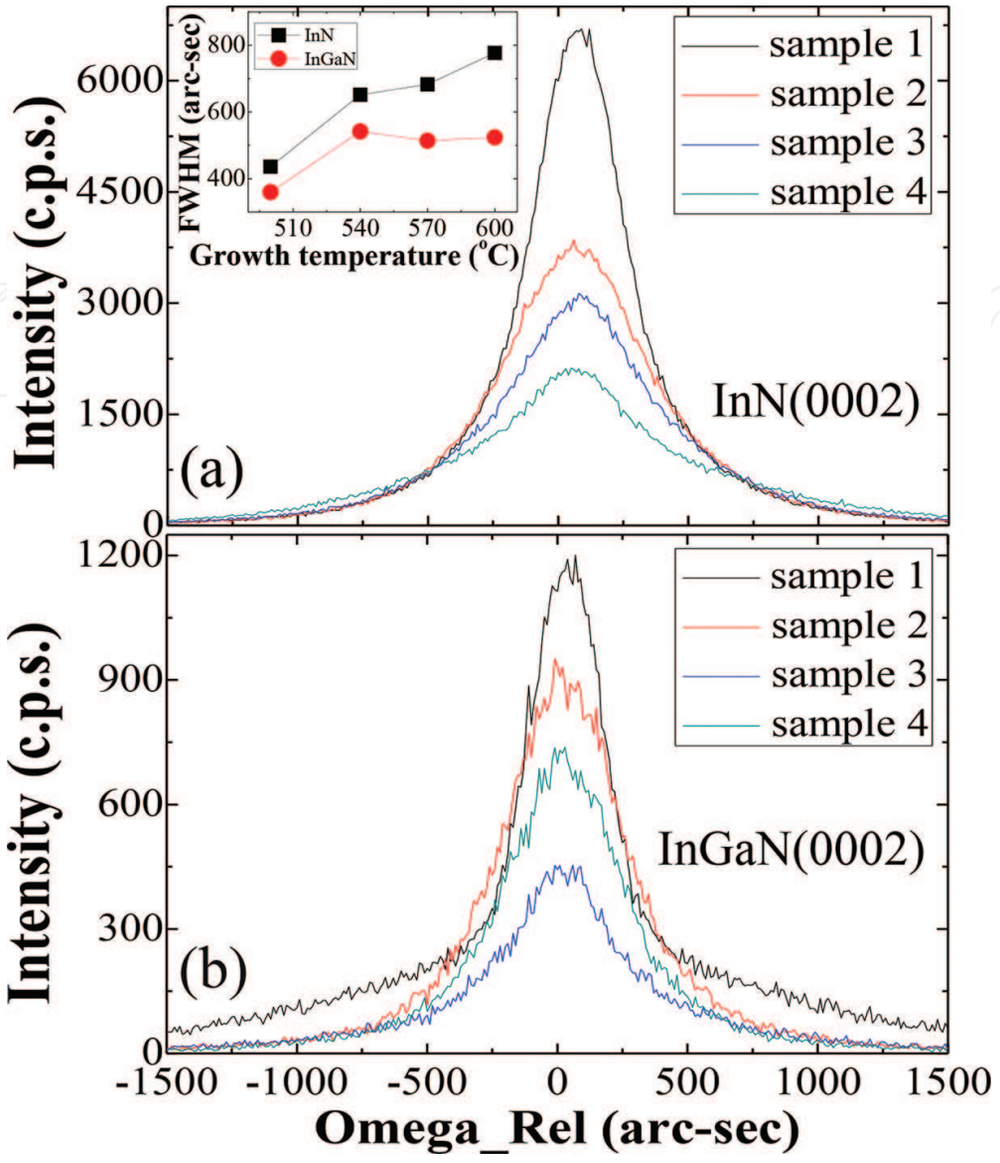

Figure 2. (a) Rocking curve of the plane of InN (0 0 0 2). (b) Rocking curve of the plane of $In_xGa_{1-x}N$ (0 0 0 2). The inset is the FWHM value vs. the growth temperature.

respectively. The FWHM values of the plane of $In_xGa_{1-x}N$ (0 0 0 2) grown on sample 1, 2, 3, and 4 are 359.6, 541.6, 513.7, and 523.8 arc-sec, respectively. It reveals that the intensity value of the plane of InN (0 0 0 2) grown on sample increases and the FWHM value of the plane of InN (0 0 0 2) grown on sample decreases with the decreasing growth temperature of InGaN grown on sample. Therefore, the maximum intensity and minimum FWHM value of the plane of InN (0 0 0 2) grown on sample 1 from **Figure 2(a)** is obtained, which shows that it is helpful to grow high-crystal quality InN epifilms by decreasing the growth temperature of the InGaN buffer layer and the growth parameter of sample 1 is suitable to grow a high-quality InN epifilm.

Figure 3(a–d) shows the surface morphology of *c*-plane (0 0 0 2) InN grown on samples 1, 2, 3, and 4, respectively, obtained by SEM (SII-3050). By comparing the RHEED patterns of InN

grown on samples 1, 2, 3, and 4 along with [1 1¯ 0 0] InN, we found that the RHEED pattern of sample 1 is streaky but others are spotty patterns, indicating that the growth mode of InN on sample 1 was established by the two-dimensional (2D) Frank-van der Merwe epitaxial growth mode. As compared to the XRD results of InN grown on sample 1 with prominent oscillations, sample 1 is a high-quality and layer-by-layer epitaxial 2D-growth sample. From SEM analysis, we observed the flatness of *c*-plane InN epifilm was getting smoother from sample 4 to sample 1 except for sample 3 because of the In drops left on the surface. The surface morphology of samples 1, 2, 3, and 4 were also analyzed by AFM with the root-mean-square (RMS) roughness, as shown in **Figure 4**. The RMS values of samples 1, 2, 3, and 4 are 0.636, 1.537, 9.821, and 1.910 nm, respectively. It shows that the surface of sample 1 is the flattest surface morphology in the samples, and supports the conclusion of XRD, RHEED, and SEM analyses. It also indicates that it is helpful to grow flat InN epifilms by decreasing the growth

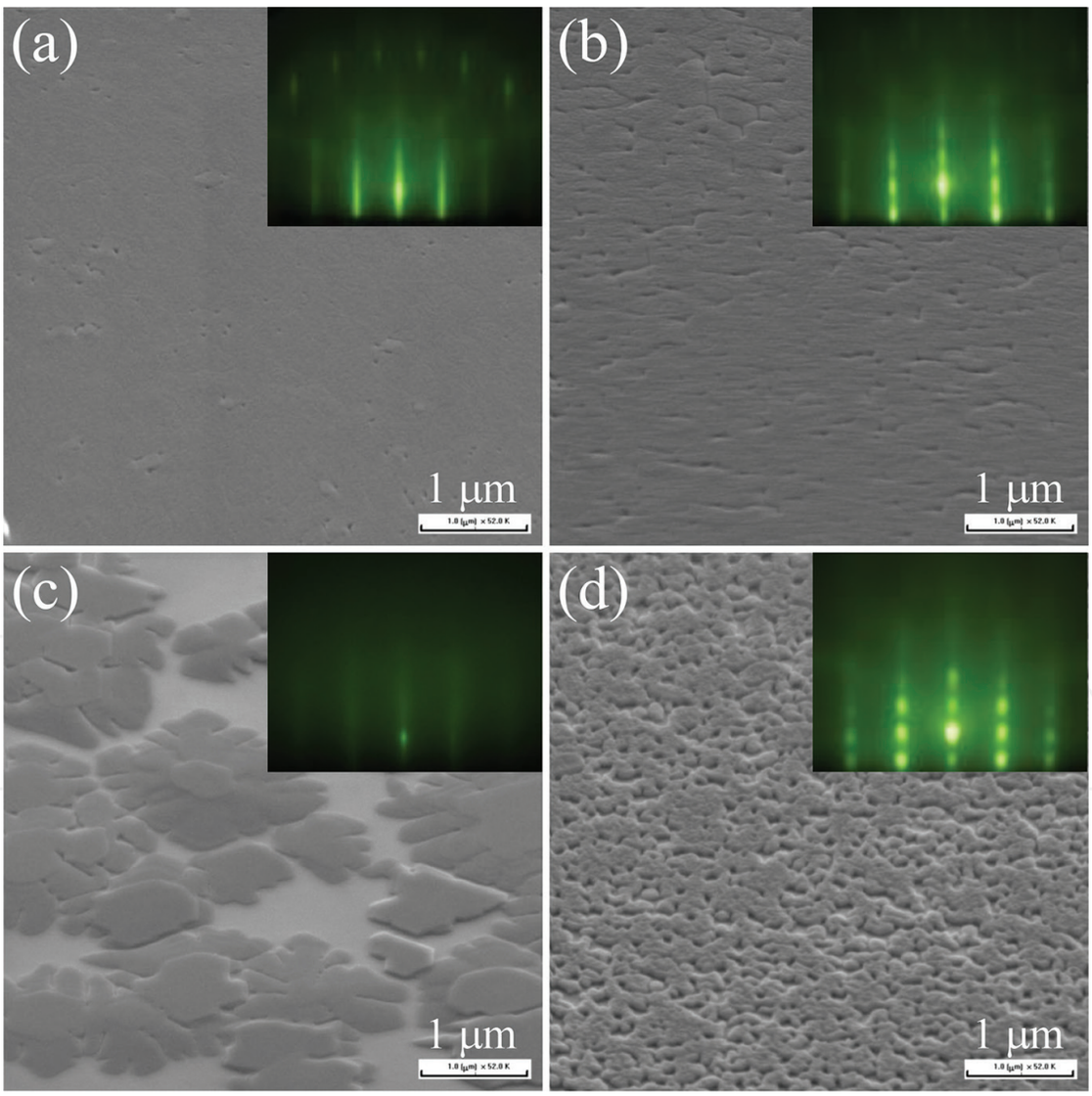

Figure 3. SEM images of *c*-plane InN thin films grown on (a) sample 1, (b) sample 2, (c) sample 3 and (d) sample 4. The scale bar is 1 μm.

http://dx.doi.org/10.5772/65812

temperature of InGaN buffer layer and the growth parameter of sample 1 offers a better condition to grow flat InN epifilms. Sample 1 was then studied in more detail.

Figure 5 shows that PL spectra of sample 1 for different temperatures. The PL measurements were carried out by Ti:sapphire laser (Traix-320) with a light source from 808-nm laser and 208 mW power from 300 to 14 K. When the temperature was changed from 300 to 14 K, the position of major peak shifted from 0.698 to 0.703 eV, in good agreement with the recent data (~0.7 eV) [7, 8]. The intensity of major peak also increased. The major peaks measured at different temperatures were confirmed by a multipeak Gaussian-function curve fitting with the software Origin (Pro. 8.0). The result of the multipeak Gaussian-function curve fitting showed that the major peak was composed by three peaks and all the peak centers shifted to higher energy when the temperature was changed from 300 to 14 K. Among three fitting peaks, only one peak can be described by Varshni's equation [21]:

$$E_g(T) = E_g(0) - \frac{\alpha T^2}{T + \beta}$$

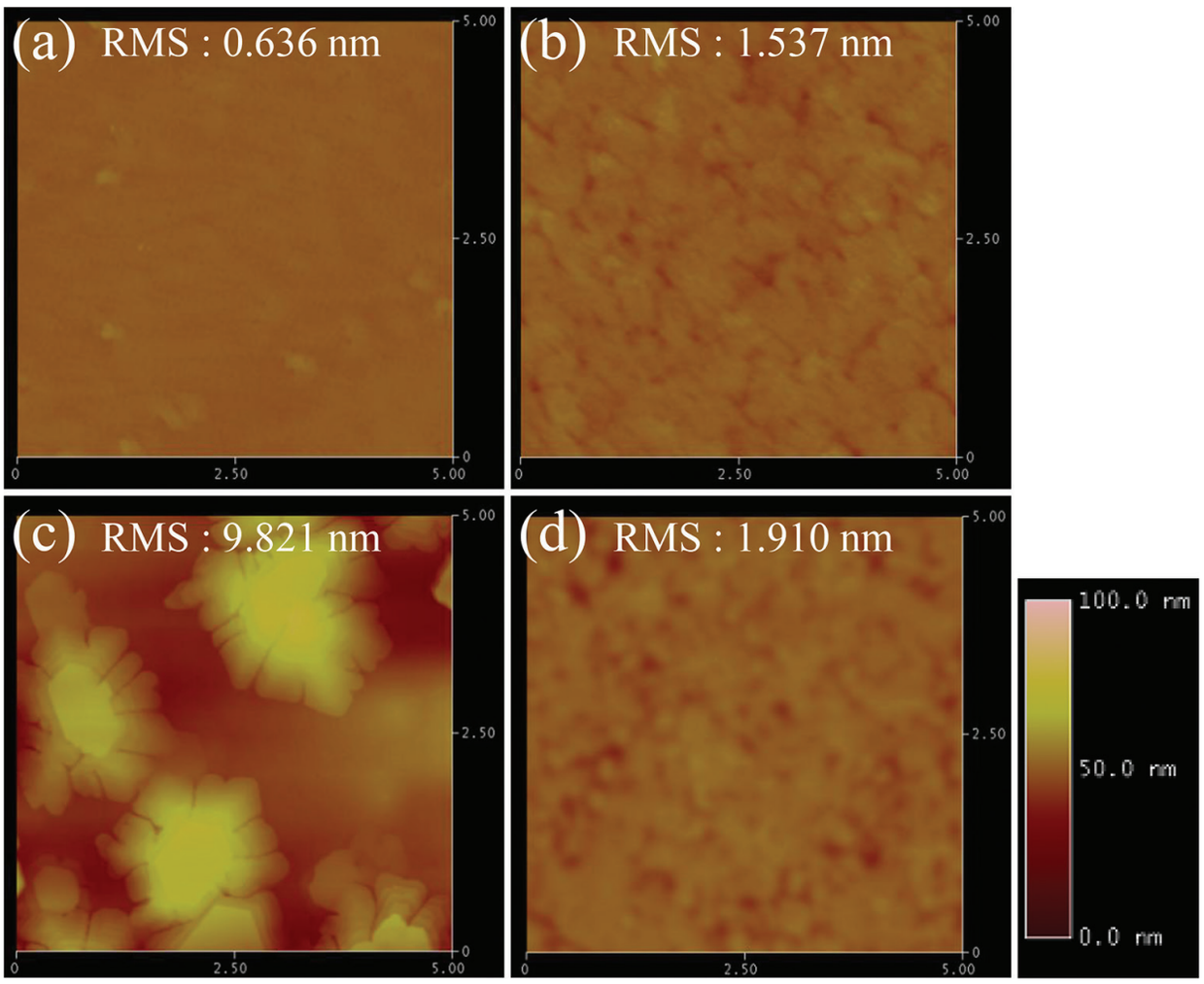

Figure 4. AFM images of surface of growing samples by 5 × 5 μm² scan: (a) sample 1, (b) sample 2, (c) sample 3, and (d) sample 4. The scale bar is 100 nm

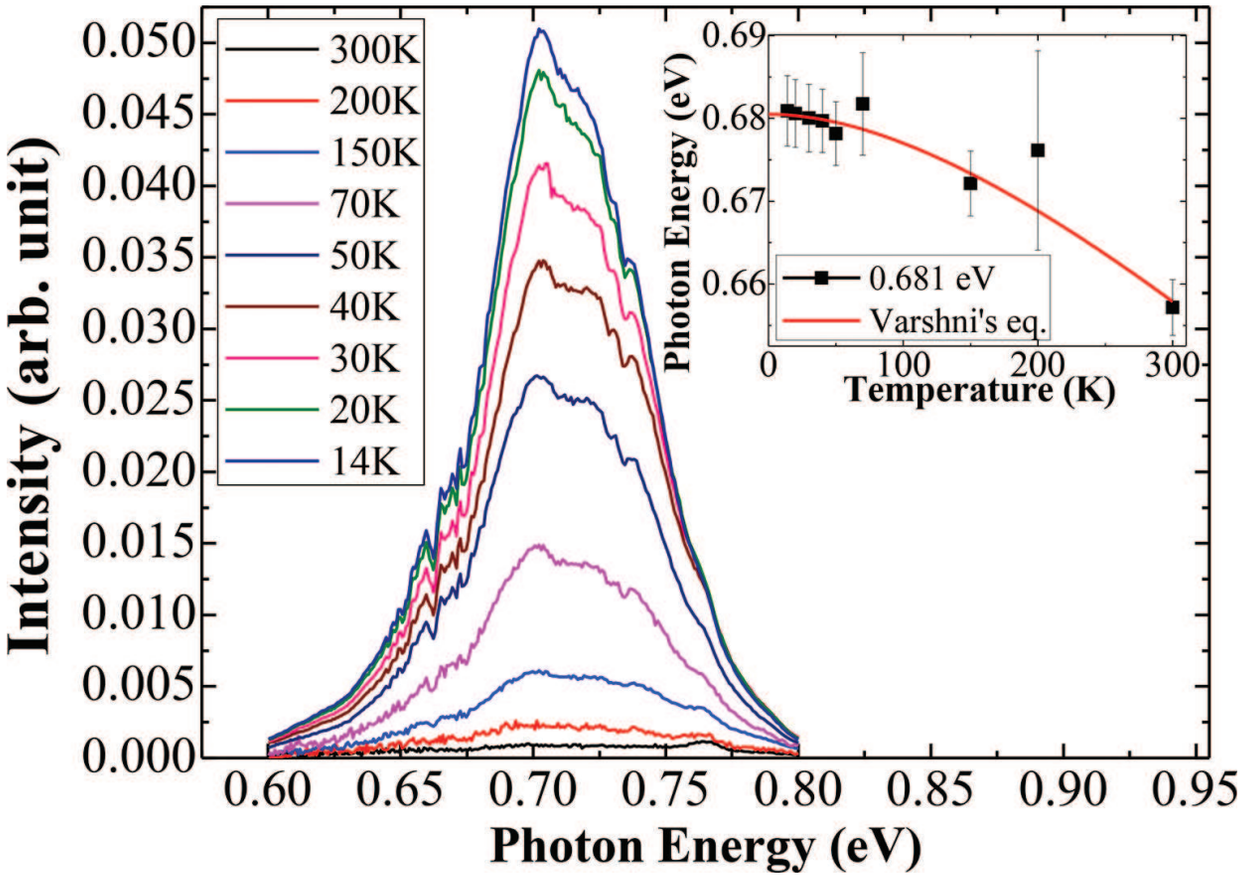

Figure 5. The PL spectra taken at different temperatures. The inset is PL peak energy as a function of temperature. The uncertainty of PL peak position is the result of the multipeak Gaussian-function curve fitting. The red curve is the theoretical fitting to Varshni's equation.

In the inset of **Figure 5**, the theoretical fitting to Varshni's equation is obtained with $E_g(0)$ = 0.681 eV, α = 0.18 meV/K and β = 416 K. As compared to $E_g(0)$ = 0.69 eV, α = 0.41 meV/K and β = 454 K from Wu et al. [8], we find that the values of $E_g(0)$ and β are consistent with the results of Wu et al., within the variation of β. The value of β, Debye temperature at 0 K, is in the range from 370 to 650 K for hexagonal InN, estimated by Davydov et al. [22]. However, the different values of α, the Varshni thermal coefficient, might be due to the different InN thicknesses of the sample used in this study. The other two peaks were nearly independent of temperature, and attributed to the defect levels.

The cross-sectional TEM specimen of sample 1 was prepared by a dual-beam focus ion beam (Seiko SII-3050), with the cleavage plane along the [1 1$^-$ 0 0] direction on the *c*-plane InN (0 0 0 1) and carbon was used as a preservation layer to avoid the damage from the Ga-ion beam during the preparation. The microstructure of sample 1 was analyzed by the field emission transmission electron microscope (FE-TEM; Phillips Tecnai F-20) with an electron voltage of 200 kV. From the TEM bright field image with [1 1 2$^-$ 0] zone axis in **Figure 6(a)**, we deduced the selective area diffraction (SAD) pattern for sample 1, as shown in **Figure 6(b)**. It shows three distinguishing rectangular diffraction spots in the SAD pattern, indicating that sample 1 was formed by the high-quality GaN, InGaN buffer layer and InN crystals. All of the spots

http://dx.doi.org/10.5772/65812

are very clear and with no distortion. It shows that there are few stacking-faults in sample 1. The ***d*-spacing** of {0 0 0 1} and {[1 1¯ 0 0]} planes of GaN were measured to be (d_{0001} = 0.5109 nm and d1 1¯ 0 0=0.2753 nm). The ***d*-spacing** of {0 0 0 1} and {[1 1¯ 0 0]} planes of InGaN were measured to be (d_{0001} = 0.5371 nm and d1 1¯ 0 0=0.2821 nm). The ***d*-spacing** of {0 0 0 1} and {[1 1¯ 0 0]} planes of InN were measured to be (d_{0001} = 0.5634 nm and d1 1¯ 0 0=0.3043 nm). This indicates that the In content of $In_xGa_{1-x}N$ in Sample 1 is, about 50% determined from these d_{0001} data, which is consistent with the XRD analysis. The scanning transmission electron microscope (STEM) measurement will show the high contract images among GaN, InGaN, and InN layers. We show the STEM result for sample 1 in **Figure 6(c)**. It clearly exhibits, with a high-resolution STEM image, that the InN epifilm was well formed on the InGaN buffer layer and the InGaN buffer layer was well established on GaN template. The thicknesses of

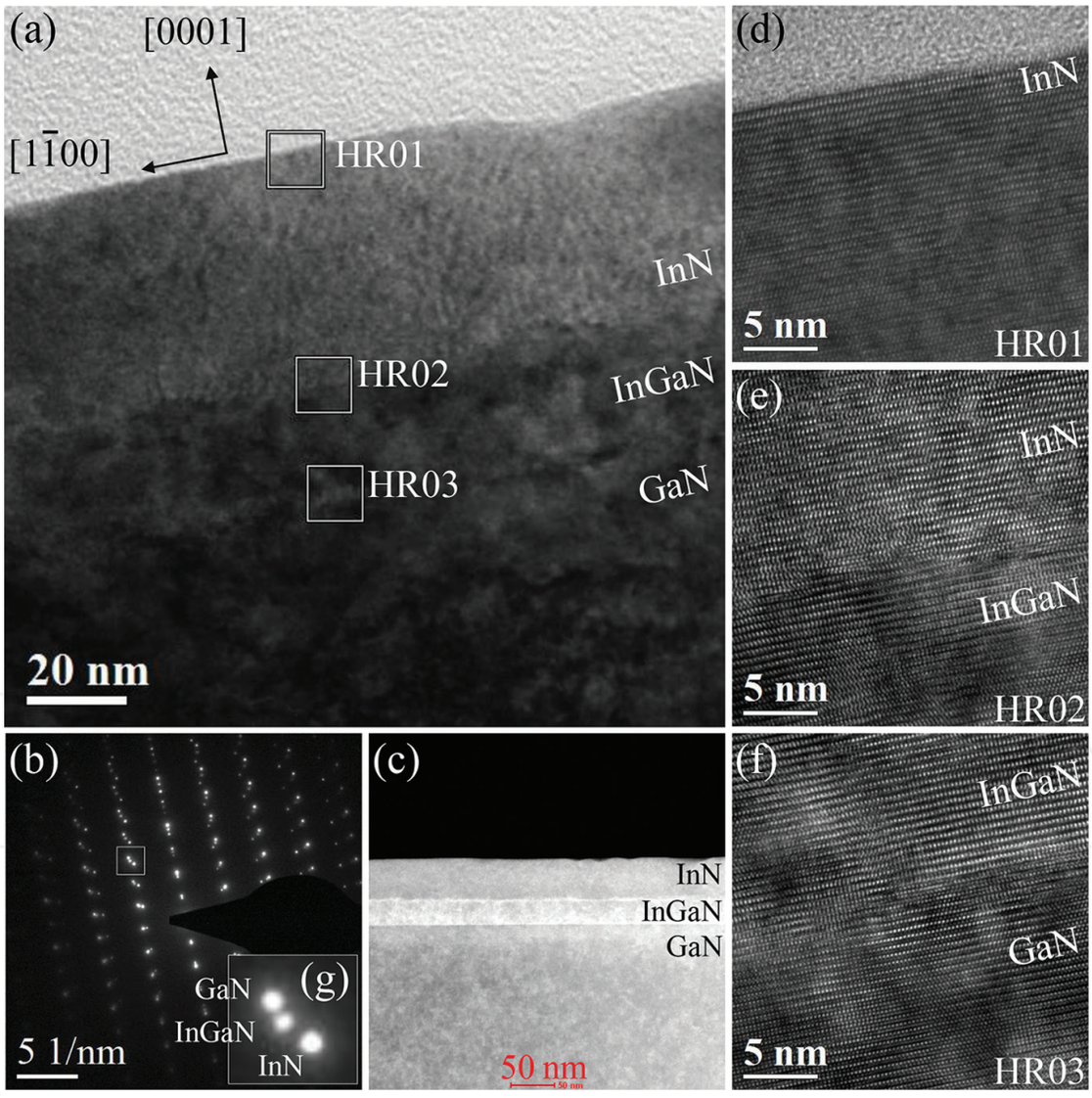

Figure 6. TEM analysis of sample 1: (a) the bright field image of TEM, the scale bar is 20 nm, (b) the selective area diffraction patterns, the scale bar is 5 (1/nm), (c) the STEM image, the scale bar is 50 nm. (d)–(f) the high-resolution TEM images of InN, InN-InGaN interface, and InGaN-GaN interface, respectively, the scale bar is 5 nm, (g) the enlarged SAD pattern of the square in (b).

InN and InGaN buffer layer were evaluated from the STEM image to be about 50 and 30 nm, respectively. The high-quality crystalline microstructures of InN, InGaN and GaN layers were also confirmed by the high-resolution TEM images. **Figure 6(d–f)** showed that InGaN buffer layer was well-stacked on GaN and high-quality InN epifilm was well-stacked on the InGaN buffer layer with some minor structural defects (e.g., dislocations or stacking faults) occurred in InN and InGaN layers.

2.4. Characteristics of InN epifilms

From the crystal structural analyses by XRD and TEM, we found that the crystal quality was significantly improved by decreasing the growth temperature of InGaN buffer layer. From the SEM images and AFM analyses, we also found that the surface of InN epifilm became smoother by decreasing the growth temperature of the InGaN buffer layer. From the PL measurements, we showed that the energy of 0.681 eV emitted from the InN epifilm of sample 1 (the growth temperature of InGaN buffer layer is 500°C) by the fitting to Varshni's equation. Finally, it is suggestive that one can grow high-quality and flat InN epifilms by decreasing the growth temperature of the InGaN buffer layer. Therefore, the influence of InGaN buffer layer is very effective to grow high-quality InN epifilms and InN microstructures as well. We therefore grow InN hexagonal microdisks on the LAO substrate with the InGaN buffer layer.

3. InN hexagonal microdisks

3.1. Growth of InN microdisks

The two-orientation growth of GaN nanopillars on the LAO substrate has been reported in our previous papers [23, 24]. In this paper, we applied the two-orientation growth to grow the 2D *M*-plane InN epifilm and 3D ***c***-plane InN hexagonal microdisks on the LAO substrate with the InGaN buffer layer at low-growth temperature (470°C). The sample was grown on a high-quality 1 × 1 cm^2 LAO (1 0 0) substrate with the InGaN buffer layer by a low-temperature PA-MBE system (Veeco Applied-GEN 930). The LAO substrate was cut from the crystal ingot, which was fabricated by the traditional Czochralski pulling technique. Then, we grew InN hexagonal microdisks with an InGaN buffer layer on the γ-$LiAlO_2$ substrate by plasma-assisted molecular beam epitaxy. The details of growth parameters can be obtained from the previous paper [25].

3.2. Analysis of InN microdisks

The crystal structure of the microdisk sample is characterized by the high-resolution X-ray diffraction (XRD; Bede D1) measurement and is shown in **Figure 7**. From the peak of X-ray diffraction pattern at 2θ = 31.69°, we estimated the content of indium of $In_xGa_{1-x}N$ on the basis of Vegard's law to be about 20% [20]. The peaks at 2θ = 29.07°, 31.31°, 32.29°, and 34.69° represent the X-ray diffraction patterns from **M**-plane InN ($1\,1^{-}\,0\,0$), ***c***-plane InN ($0\,0\,0\,2^{-}$),

http://dx.doi.org/10.5772/65812

M-plane GaN (1 1^{-} 0 0) and LAO (1 0 0), respectively. By the asymmetric double sigmoidal linear curve fitting with the software Quick Graph (version 2.0), these XRD peak positions were obtained that agreed with those data of the standard wurtzite structure bulk InN (JCPDS file No. 50-1239). The ***d*-spacing** between {0 0 0 2^{-}} planes of InN was evaluated to be d_{0002} = 0.28216 nm from the Bragg's law ($2d\sin\theta = n\lambda$) with Cu K_α wavelength λ = 0.1540562 nm. The lattice constant of wurtzite InN microdisk is smaller than that of bulk InN by 1.09%, as compared with the value on JCPDS file, d_{0002} = 0.28528 nm.

The surface morphology of the sample was evaluated by the field emission scanning electron microscope (FE-SEM, SII-3050). **Figure 7(a)** showed the top-view SEM image of the sample. The morphology of the sample exhibited that 3D ***c***-plane InN hexagonal microdisks and 2D ***M***-plane InN epifilm were grown on the LAO substrate. **Figure 7(b)** showed the tilt-view SEM image of the InN microdisk shown in the center of **Figure 7(a)**, and the diameter of the InN microdisk was 0.60 μm. The micrographic image of the sample showed that the 3D ***c***-plane InN hexagonal microdisks and nanopillars were grown atop an anionic hexagonal basal plane of LAO, while the 2D ***M***-plane InN epifilm were developed along with the lateral orientation [112^{-}0]InN//[001]LAO.

The microstructure of the sample was analyzed by a field emission transmission electron microscope (FE-TEM; Phillips Tecnai F-20) at an electron voltage of 200 kV. The cross-sectional TEM specimen was prepared by a dual-beam focus ion beam (FIB; Seiko SII-3050), on the

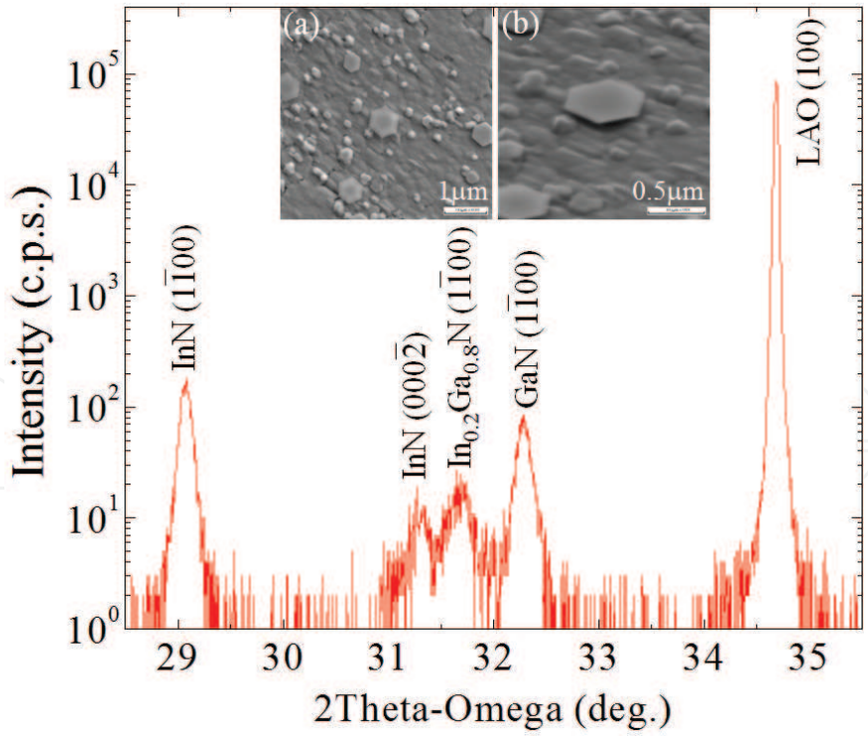

Figure 7. The X-ray 2 Theta-Omega scan of the sample. In the inset of (a) the top-view SEM image of the sample, the scale bar is 1 μm. (b) Enlarged SEM image with a tilted angle of InN hexagonal thin disk, the scale bar is 0.5 μm.

cleavage plane along [11¯00] direction of the ***c***-plane InN hexagonal thin disk. **Figure 8(a)** showed the bright field image with [112¯0]InN//[001]LAO zone axis. The thicknesses of ***M***-plane InN, ***M***-plane InGaN and ***M***-plane GaN were measured to be about 265, 51, and 137 nm, respectively. The height for the ***c***-plane InN hexagonal thin disk from neck to top was about 188 nm. The high-resolution TEM images with [112¯0]InN//[001]LAO zone axis were performed in the areas HR01 and HR02 of the sample, as shown in **Figure 8(a)**. From high-resolution TEM analyses, we found the staking faults at the boundary between ***M***-plane and ***c***-plane GaN, which released the strains between the misfit ***M***-plane and ***c***-plane wurtzite structures of GaN and InGaN. The *c*-plane wurtzite structure was followed up to the neck area and formed a uniform ***c***-plane InGaN pyramid-shaped structure. The wave-shaped InN was produced by the staking faults between the misfit ***c***-plane wurtzite structures of InGaN and InN. In **Figure 8(b)**, the wave-shaped InN became uniform in the area HR01 and followed further to form the InN hexagonal thin disk structure. In **Figure 8(c)**, the high-quality crystalline structure of the InN thin disk is shown in the area HR02. **Figure 8(d–i)** shows the selective area diffraction (SAD) patterns taken along the growth direction from the bottom to the top (labeled from DP01 to DP06), which covered ***c***-plane GaN, ***M***-plane GaN, ***c***-plane InN, and ***M***-plane InN. **Figure 8(d)** simply shows one clear single rectangular diffraction pattern (white) at the location of DP03, indicating that the hexagonal thin disk was uniquely formed by the ***c***-plane wurtzite InN crystal. The ***d*-spacing** between {0 0 0 1¯} planes and {1 1¯ 0 0} planes of InN hexagonal thin disk were measured to be ***dc*** = 0.5687 nm and ***dM*** = 0.3025 nm, respectively. Compared with the values given in JCPDS file No. 50-1239 which are 0.5703 and 0.30647 nm, respectively, the difference between wurtzite InN thin disk and bulk InN for ***dc*** and ***dM*** are 0.28 and 1.24%, respectively, revealing that the

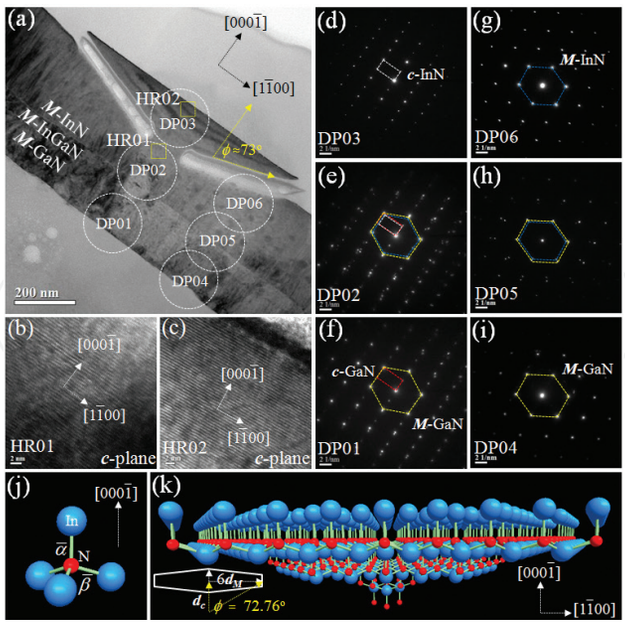

Figure 8. TEM analyses of the InN hexagonal thin disk: (a) the bright field image with [1 1 2¯ 0]InN//[0 0 1]LAO zone axis. The high-resolution TEM images taken at the points shown in (a) are presented in (b) and (c), the scale bar is 2 nm. The selective area diffraction patterns taken at the points shown in (a) are presented in [(d) – (i)], the scale bar is 2 (1/nm). The ball-stick model for InN epilayer: (j) the chemical bonds of (0 0 0 1¯) surface, (k) the hexagonal thin disk.

lattice constant of InN thin disk is smaller than that of bulk InN. The result is consistent with the XRD analysis. In **Figure 8(e)**, the SAD patterns showed the overlapping diagram of two rectangles and two hexagons at the neck area of the disk (location of DP02), indicating that a ***c***-plane InN (white rectangle) was formed in addition to the ***c***-plane GaN (red rectangle), ***M***-plane InN (blue hexagon), and ***M***-plane GaN (yellow hexagon) at the neck area. We checked the ***M***-plane InN (blue hexagon) and ***M***-plane GaN (yellow hexagon) by the SAD patterns, as shown in **Figure 8(g–i)**. These two hexagons are identical to those shown in **Figure 8(h)**, indicating that the ***M***-plane wurtzite InN and ***M***-plane wurtzite GaN were grown in the same crystalline direction. From the analyses of SAD patterns, we found that the ***c***-plane wurtzite nanocrystal was embedded between ***M***-plane wurtzite nanocrystal areas at the beginning of nucleation when GaN was grown on the LAO substrate. We demonstrated a ball-stick model for the self-assembled InN hexagonal thin disk to establish the growth mechanism of the InN hexagonal thin disk. The ball-stick model for the standard wurtzite InN (JCPDS file No. 50-1239) with $\boldsymbol{a} = \boldsymbol{b} = 0.3537$ nm, $\boldsymbol{c} = 0.5703$ nm, and $u=\alpha^{-}/c= 3/8$ was used to simulate the ***c***-plane InN thin disk in **Figure 8(j)**, where blue balls and red balls represented In atoms and N atoms, respectively. In our previous paper, we showed that the GaN $(0\,0\,0\,1^{-})$ microdisk with a tilted angle of $\theta = \tan^{-1}(\boldsymbol{dM}/\boldsymbol{dc}) = 28°$ was established with the capture of N atoms by the β^{-}-dangling bonds of the most-outside Ga atoms for each ***dc*-spacing** during the GaN lateral overgrowth [5]. In the case of InN thin disk, when the growth temperature was lowered to 470°C, the ***c***-plane InN $(0\,0\,0\,1^{-})$ hexagonal thin disk was built up with the capture of N atoms by the β^{-}-dangling bonds of the most-outside In atoms and then the lateral overgrowth occurred; by capture of In atoms by β^{-}-dangling bonds of N atoms, to form the thin disk. The lateral overgrowth along the $(1\,1^{-}\,0\,0)$ direction was extended to six ***dM*-spacings** for each ***dc*-spacing**, resulting in the angle of 73 off the ***c***-axis. Based on the ball-stick model, the edge was then tilted off the *c*-axis $[0\,0\,0\,1^{-}]$ direction by the angle of $\varphi = \tan^{-1}(6\boldsymbol{dM}/\boldsymbol{dc}) = 72.76°$ as shown in **Figure 8(k)**. We also calculated the angle from the measured SAD data at the InN hexagonal thin disk in **Figure 8(d)**, and obtained that the *d*-spacing between $\{0\,0\,0\,1^{-}\}$ planes was $\boldsymbol{dc} = 0.5687$ nm and the ***d*-spacing** between $\{1\,1^{-}\,0\,0\}$ planes was $\boldsymbol{dM} = 0.3025$ nm, resulting in $\varphi = \tan^{-1}(6\boldsymbol{dM}/\boldsymbol{dc}) = 72.60°$, which was in good agreement with the model predicted.

3.3. Characteristics of InN microdisks

We have grown InN hexagonal thin microdisks on the LAO substrate with the InGaN buffer layer by PA-MBE. From the SEM images and TEM analyses, we found that ***c***-plane wurtzite was established at the nucleation of GaN on the LAO substrate and ***c***-plane InN hexagonal thin disks were built up at low temperature (470°C) after insetting the InGaN buffer layer. The ***c***-plane InN $(0\,0\,0\,1^{-})$ hexagonal thin disk was produced with the capture of N atoms by the β^{-}-dangling bonds of the most-outside In atoms, and then laterally over-grown along $[1\,1^{-}\,0\,0]$ direction by six ***dM*-spacings** for each ***dc*-spacing**. The oblique angle of InN hexagonal thin disk was formed by the lateral overgrowth of the wurtzite structure. Based on the standard wurtzite InN, the angle of $\varphi = \tan^{-1}(6\boldsymbol{dM}/\boldsymbol{dc}) = 72.76°$ was evaluated. The oblique angle of InN hexagonal thin disk can be examined directly from the SAD pattern and high-resolution TEM analyses to be 72.60° and about 73°, respectively.

4. Conclusion

In this paper, we have reported the growth and characteristics of 2D *c*-plane InN (0 0 0 1) epifilms and 3D *c*-plane InN (0 0 0 1^{-}) hexagonal thin microdisks with InGaN buffer layers at low temperatures by PA-MBE. By decreasing the growth temperature of the InGaN buffer layer, we can grow high-quality and flat InN epifilms. Besides, InGaN buffer layer can also provide the growth base to form InN hexagonal thin microdisks. By introducing InGaN buffer layers, the high-quality InN epifilms and microstructures can be grown under suitable growth conditions. Consequently, the InN hexagonal thin microdisk provides an opportunity to fabricate the InGaN/GaN microdisk quantum well for the application of full-color micron LED.

Acknowledgements

The project was supported by the Ministry of Science and Technology of Taiwan and the Core Facilities Laboratory for Nanoscience and Nanotechnology in Kaohsiung and Pintung Area.

Author details

Chen-Chi Yang[1,2], Ikai Lo[1,2]*, Cheng-Hung Shih[1,2], Chia-Hsuan Hu[1,2], Ying-Chieh Wang[1,2], Yu-Chiao Lin[1,2], Cheng-Da Tsai[1,2], Hui-Chun Huang[1,2], Mitch M. C. Chou[1,2], Cheng-Chang Yu[1,2] and Der-Jun Jang[1,2]

*Address all correspondence to: ikailo@mail.phys.nsysu.edu.tw

1 Department of Physics, Center for Nanoscience and Nanotechnology, National Sun Yat-Sen University, Kaohsiung, Taiwan

2 Department of Materials and Optoelectronics Science, National Sun Yat-Sen University, Kaohsiung, Taiwan

References

[1] S. Nakamura, M. Senoh, N. Iwasa, S. I. Nagahama, T. Yamada, and T. Mukai. Super-bright green InGaN single-quantum-well-structure light-emitting diodes. Japanese Journal of Applied Physics. 1995;**34**(Part 2, Number 10B):L1332-L1335. DOI: 10.1143/JJAP.34.L1332

[2] S. Nakamura, S. Pearton, and G. Fasol, editors. The Blue Laser Diode: The Complete Story. Berlin: Springer Science & Business Media; 20 0 0 . 367 p. DOI: 10.1007/978-3-662-04156-7

[3] I. Lo, J. K. Tsai, W. J. Yao, P. C. Ho, L. W. Tu, T. C. Chang, S. Elhamri, W. C. Mitchel, K. Y. Hsieh, J. H. Huang, H. L. Huang, and W. C. Tsai. Spin splitting in modulation-doped

Al_xGa_{1-x} N/GaN heterostructures. Physics Review B. 2002;**65**:161306. DOI: 10.1103/PhysRevB.65.161306

[4] I. Lo, W. T. Wang, M. H. Gau, J. K. Tsai, S. F. Tsay, and J. C. Chiang. Gate-controlled spin splitting in GaN/AlN quantum wells. Applied Physics Letters. 2006;**88**:082108. DOI: 10.1063/1.2178505

[5] I. Lo, C. H. Hsieh, Y. C. Hsu, W. Y. Pang, and M. C. Chou. Self-assembled GaN hexagonal micropyramid and microdisk. Applied Physics Letters. 2009;**94**:062105. DOI: 10.1063/1.3079078

[6] A. Y. Cho, and J. R. Arthur. Molecular beam epitaxy. Progress in Solid State Chemistry. 1975;**10**, Part 3:157-191. DOI: 10.1016/0079-6786(75)90 0 0 5-9

[7] J. Wu, W. Walukiewicz, K. M. Yu, J. W. Ager III, E. E. Haller, H. Lu, W. J. Schaff, Y. Saito and Y. Nanishi. Unusual properties of the fundamental band gap of InN. Applied Physics Letters. 2002;**80**:3967. DOI: 10.1063/1.1482786

[8] J. Wu, W. Walukiewicz, W. Shan, K.M. Yu, J.W. Ager, S.X. Li, E.E. Haller, H. Lu, and W.J. Schaff. Temperature dependence of the fundamental band gap of InN. Journal of Applied Physics. 2003;**94**:4457-4460. DOI: 10.1063/1.1605815

[9] S. K. O'Leary, B. E. Foutz, M. S. Shur, U. V. Bhapkar, and L. F. Eastman. Electron transport in wurtzite indium nitride. Journal of Applied Physics. 1998;**83**:826-829. DOI: 10.1063/1.366641

[10] Z. Y. Fan and N. Newman. Experimental determination of the rates of decomposition and cation desorption from AlN surfaces. Material Science Engineering: B. 2001;**87**:244-248. DOI: 10.1016/S0921-5107(01)00720-6

[11] C. H. Liang, L. C. Chen, J. S. Hwang, K. H. Chen, Y. T. Hung, and Y. F. Chen. Selective-area growth of indium nitride nanowires on gold-patterned Si(1 0 0) substrates. Applied Physics Letters. 2002;**81**:22-24. DOI: 10.1063/1.1490636

[12] T. Stoica, R. Meijers, R. Calarco, T. Richter, and H. Luth. MBE growth optimization of InN nanowires. Journal of Crystal Growth. 2006;**290**:241-247. DOI: 10.1016/j.jcrysgro.2005.12.106

[13] Y. L. Chang, F. Li, A. Fatehi, and Z. Mi. Molecular beam epitaxial growth and characterization of non-tapered InN nanowires on Si (1 1 1). Nanotechnology. 2009;**20**:345203. DOI: 10.1088/0957-4484/20/34/345203

[14] I. Lo, Y. C. Wang, Y. C. Hsu, C. H. Shih, W. Y. Pang, S. T. You, C. H. Hu, M. M. C. Chou, and G. Z. L. Hsu. Electrical contact for wurtzite GaN microdisks. Applied Physics Letters. 2014;**105**:082101. DOI: 10.1063/1.4894080

[15] K. Xu and A. Yoshikawa. Effects of film polarities on InN growth by molecular-beam epitaxy. Applied Physics Letters. 2003;**83**:251-253. DOI: 10.1063/1.1592309

[16] H. Xiao, X. Wang, J. Wang, N. Zhang, H. Liu, Y. Zeng, J. Li, and Z. Wang. Growth and characterization of InN on sapphire substrate by RF-MBE. Journal of Crystal Growth. 2005;**276**:401-406. DOI: 10.1016/j.jcrysgro.2004.12.001

[17] Y. Saito, T. Yamaguchi, H. Kanazawa, K. Kano, T. Araki, Y. Nanishi, N. Teraguchi, and A. Suzuki. Growth of high-quality InN using low-temperature intermediate layers by RF-MBE. Journal of Crystal Growth. 2002;237-239:1017-1021. DOI: 10.1016/S0022-0248(01)02119-4

[18] H. Lu, W. J. Schaff, J. Hwang, H. Wu, G. Koley, and L. F. Eastman. Effect of an AlN buffer layer on the epitaxial growth of InN by molecular-beam epitaxy. Applied Physics Letters. 2001;79:1489-1491. DOI: 10.1063/1.1402649

[19] J-K. Tsai, I. Lo, K-L. Chuang, L-W.Tu, J-H. Huang, C-H. Hsieh, and K-Y. Hsieh. Effect of N to Ga flux ratio on the GaN surface morphologies grown at high temperature by plasma-assisted molecular-beam epitaxy. Journal of Applied Physics. 2004;**95**:460. DOI: 10.1063/1.1634388

[20] A. R. Denton and N. W. Ashcroft. Vegard's law. Physical Review A. 1991;**43**:3161-3164. DOI: 10.1103/PhysRevA.43.3161

[21] Y.P. Varshni. Temperature dependence of the energy gap in semiconductors. Physica. 1967;34:149-154. DOI: 10.1016/0031-8914(67)90062-6

[22] V. Yu. Davydov, V. V. Emtsev, I. N. Goncharuk, A. N. Smirnov, V. D. Petrikov, V. V. Mamutin, V. A. Vekshin, S. V. Ivanov, M. B. Smirnov and T. Inushima. Experimental and theoretical studies of phonons in hexagonal InN. Applied Physics Letters. 1999;**75**:3297-3299. DOI: 10.1063/1.125330

[23] C. H. Hsieh, I. Lo, M. H. Gau, Y. L. Chen, M. C. Chou, W. Y. Pang, Y. I. Chang, Y. C. Hsu, M. W. Sham, J. C. Chiang, and J. K. Tsai. Self-assembled c-plane GaN nanopillars on γ-$LiAlO_2$ substrate grown by plasma-assisted molecular-beam epitaxy. Japanese Journal of Applied Physics. 2008;**47**:891-895. DOI: 10.1143/JJAP.47.891

[24] I. Lo, C. H. Hsieh, Y. L. Chen, W. Y. Pang, Y. C. Hsu, J. C. Chiang, M. C. Chou, J. K. Tsai, and D. M. Schaadt. Line defects of M-plane GaN grown on g-$LiAlO_2$ by plasma-assisted molecular beam epitaxy. Applied Physics Letters. 2008;**92**:202106. DOI: 10.1063/1.2924288

[25] C. C. Yang, I. Lo, C. H. Hu, H. C. Huang, and M.M. C. Chou. Growth of InN hexagonal microdisks. AIP Advances. 2016;**6**:085015. DOI: 10.1063/1.4961699